Radiative-convective equilibrium using GCM column physics

Isaac M. Held
Geophysical Fluid Dynamics Laboratory / NOAA Princeton University Forrestal Campus / US Route 1 P.O.Box 308 Princeton, New Jersey 08542

Ming Zhao
Program in Atmospheric and Oceanic Sciences, Department of Geosciences, Princeton University, Princeton, New Jersey, USA

Bruce Wyman
Geophysical Fluid Dynamics Laboratory / NOAA Princeton University Forrestal Campus / US Route 1 P.O.Box 308 Princeton, New Jersey 08542

To be submitted to: Journal of the Atmospheric Sciences

Corresponding author address:
Dr. Isaac M. Held, Geophysical Fluid Dynamics Laboratory / NOAA Princeton University Forrestal Campus / US Route 1
P.O.Box 308 Princeton
New Jersey 08542

Abstract.

The behavior of a GCM column physics package in a non-rotating, doubly periodic, homogeneous setting with prescribed SSTs is examined. This radiative-convective framework is proposed as a useful tool for studying the effects of differing modeling assumptions on convective organization and cloud feedbacks.

For the column physics utilized here, from GFDL's AM2 model, many of the properties of the homogeneous, non-rotating model are closely tied to the fraction of precipitation that is large-scale, rather than convective. Significant large-scale precipitation appears above a critical temperature and then increases with further increases in temperature. The amount of large-scale precipitation is a function of horizontal resolution and can also be controlled by modifying the convection scheme, as we illustrate by modifying assumptions concerning entrainment into convective plumes. Some similarities and some differences are found between the behavior of the homogeneous model and that of the tropics of the parent GCM when ocean temperatures are increased and when the convection scheme is modified.

1. Introduction

When trying to understand the differences between atmospheric climate simulations, one needs to evaluate the significance of a myriad of assumptions concerning moist convection, boundary layer mixing, and cloud prediction, and the manner in which these interact with each other, with radiative transfer, with the land surface, and with the dynamical core of the model. It is our belief that this work would benefit significantly from the development of more idealized contexts in which one can study the implications of these modeling assumptions. In this paper we explore the possibility of using radiative-convective equilibrium as such an idealized framework. The claim is that it is of interest to take the full GCM physics package and couple it with non-rotating hydrostatic dynamics in a doubly-periodic box, over a uniform SST boundary condition, and examine the resulting statistically steady state, using comparable horizontal and vertical resolution to the parent GCM. One can examine the sensitivity of a control simulation to different aspects of the closure schemes and to resolution. One can also examine how the response to a change in the SSTs is modified by these choices.

It may seem odd to examine radiative-convective equilibrium in a hydrostatic model at GCM resolution when there is a flourishing activity using non-hydrostatic models at cloud-resolving resolutions for this purpose (e.g., Tompkins and Craig 1999; Tao et al. 1999). See Larson and Hartmann (2003) for an example of radiative-convective equilibrium in a model with parameterized convection, albeit at somewhat higher, mesoscale, resolutions than those considered here. We argue that idealized models using a GCM's resolution and physics package are themselves objects worthy of study, especially if that GCM is being used to make climate change predictions that help form the basis for society's response to global warming.

We base this study on the AM2 physics described in Anderson et al. (2004). We find a host of interesting sensitivities in this physics package, but do not try to describe most of these here. Rather we focus on one result that illustrates the utility of this methodology: we find that the model behavior in this configuration is strongly dependent on whether or not any "gridpont storms" are generated, within which the rainfall is large-scale rather than convective. This

aspect of the solution is sensitive to the manner in which entrainment rates are constrained in the convection scheme, and is also sensitive to horizontal resolution. We also refer to the results with the full spherical AM2 model with realistic boundary conditions, including perturbation experiments in which SSTs are increased 2K everywhere, to examine the extent to which results from this homogeneous non-rotating geometry do or do not carry over to realistic configurations of the model. We present some results in which we add a large-scale wind speed to the surface flux computation in the radiative-convective model, because it appears that by desensitizing the evaporation to changes in convective organization one can, in some cases, improve the similarity between the idealized radiative-convective model and the parent GCM.

2. The model

Our base model is AM2p12b, the version of the model described in Anderson et al. (2004). With a few changes in the tuning of the cloud scheme, this is the atmospheric component of CM2.0 (Delworth et al. 2005) and is referred to as AM2.0 in that context. This is a grid point GCM, so we can utilize the same code base as the full GCM, removing the spherical geometry and rotation, and introducing periodic boundary conditions in latitude as well as longitude, thereby insuring that the model is as close to the full GCM as possible. We hope to compare to results with the finite-volume core used in CM2.1 in the near future.

For our standard model we use AM2's vertical grid with 24 levels, and a 64x64 grid with 222 km resolution, comparable to AM2's 2x2.5 degree resolution near the equator. We also describe results with a model of twice the horizontal resolution (111km) using a 128x128 domain of the same physical size.

The radiative forcing is configured using an equatorial annual mean solar zenith angle. There is no diurnal cycle. All surface parameters are taken from the GCM's prescription over an ocean surface. There are no aerosols in the atmosphere. The ozone profile is specified at annual mean equatorial values, while the CO_2 concentration is 355 ppm. The model is initialized with a typical tropical sounding plus small random noise in the temperatures, but the only part of this initial

condition that is relevant to the final statistically steady state of the model is the stratospheric water vapor. All of our integrations are for 550 days, starting with the same initial condition, and averaged over the final 500 days. Equilibration times for stratospheric water, especially in a model without large-scale circulation in the stratosphere, are far longer than this, so the stratospheric water effectively remains at its initial value. The lack of equilibration in the stratosphere might have significant effects in a model in which SSTs are predicted. We do not believe that they are significant here, with fixed SSTs, but we have not investigated this dependence directly. There is no imposed "large-scale upward motion" that is often used to drive cloud-resolving models.

Cloud resolving simulations in this geometry have raised some questions concerning robustness. In 2 dimensional (x-z) simulations the convection tends to clump and continuously reside in the same small fraction of the domain, with the rest of the domain progressively drying due to subsidence (e.g., Held et al. 1993). This clumping behavior can be eliminated by adding small vertical shears to the mean zonal flows so as to redistribute vapor horizontally. The hope has been that this behavior is not present in 3D, but recent calculations in larger domains for longer times suggest that this lack of homogeneity remains an issue (Bretherton et al. 2005). In our low resolution simulations, the flow equilibrates statistically within 50 days, and we have found no dramatic dependence on the size of the domain or of inhomogeneity that grows with time. We impose no horizontal winds on the flow.

We realize that transplanting the model physics to this doubly periodic geometry will not always be straightforward, especially with spectral models. As an alternative to reconfiguring the model geometry, one can simply solve for homogeneous non-rotating radiative-convective equilibrium on the sphere, using the same SSTs and identical radiative forcing at all points. The results should be horizontally homogeneous and essentially identical to those obtained in the doubly periodic geometry, as long as scales comparable to the radius of the earth do not come into play. We have obtained such solutions using AM2 and find that the results are indeed quite similar to the doubly periodic case away from the poles (see Fig 1); however, the inhomogeneity of the grid near the poles causes the convection to be inhomogeneous. In fact, the differences in

the convection at the poles as compared to the equator are qualitatively similar to those that occur when the resolution is increased in the doubly-periodic model (as described in the following). Non-rotating spherical homogeneous radiative-convective equilibrium is an interesting test of the homogeneity of one's numerical scheme on the sphere, but we do not pursue this issue here.

Since the problem posed is horizontally homogeneous, there is a solution in which identical convection occurs at each grid point, with identically zero resolved motions. This solution is unstable in all cases examined. Studying the character of this instability is made more complex by the fact that when we compute single column radiative-convective equilibrium of parameterized convection we invariably generate a quasi-periodic time-dependent solution, rather than a steady state. There is no hint of this periodicity in our full solutions. The dynamic radiative-convective equilibria described here are more relevant to the behavior of the full GCM than are these unstable single-column solutions.

The convective closure in the model is a modified version of the Relaxed Arakawa-Schubert (RAS) scheme of Moorthi and Suarez (1992). As in Arakawa and Schubert (1974), the scheme is based on a kinematic picture of convection consisting of an ensemble of entraining plumes characterized by different lateral entrainment rates λ, with detrainment limited to the top of the plume. The λ's are determined by computing the values needed to produce plumes which attain their levels of neutral buoyancy at each model level. Starting with the shallowest plume, one checks that its cloud work function (the kinetic energy available to the entraining plume) is larger than a prescribed critical value. One then computes its mass flux by relaxing its cloud work function to its critical value on a prescribed time scale, both the critical cloud work function and the relaxation time being functions of the depth of the convection. One modifies the grid box temperature and moisture fields, and then moves on to the next plume, which rises through the column as modified by the shallower plume. One continues this process for all allowed plumes. The scheme handles both shallow and deep convection.

A detail of the convection scheme, related to the spectrum of entrainment rates, plays a role in the discussion to follow. AM2 uses a version of RAS in which a non-entraining plume is added

to this spectrum, the intention being to improve the convergence properties of the model when the vertical resolution in the upper troposphere is marginal (M. Suarez, personal communication). Unlike the other plumes in the spectrum, the non-entraining plume typically detrains into two layers rather than one, since its level of neutral buoyancy does not correspond to a model grid point. While this point did not come into focus until late in the development process, it turns out that it is not just the deep convection but also the shallow convection in the model that is sensitive to the addition of the non-entraining plume to the spectrum.

Following Tokioka et al. (1988), it was found that disallowing all plumes with entrainment rates smaller than a critical value λ_0 has advantageous effects on deep convection in the model, especially in regard to transient eddies in the tropics. Any value of λ_0 greater than 0 eliminates the non-entraining plume. But because the model's shallow convection and cloud distribution is strongly influenced by the non-entraining plume, the expedient but arbitrary choice was made in the development of AM2 to restrict the application of this entrainment limiter to deep convection ($>$ 500 mb top) to avoid strongly affecting low level cloudiness and the model's energy balance. As in Tokioka et al. (1988), we set $\lambda_0 = \alpha/z_M$, where α is non-dimensional (0.025 in the standard model) and z_M is the depth of the subcloud layer. Given our implementation, increasing α makes it more difficult for deep convection to occur, especially in dry environments in which plumes lose buoyancy rapidly when entraining, while leaving shallow convection unaltered. As $\alpha \to \infty$, parameterized deep convection becomes impossible, and grid-scale condensation and ascent must occur to heat the upper troposphere and balance radiative cooling. By varying α one modifies the fraction of precipitation that occurs through the large scale cloud/condensation module as opposed to the convection module. The large-scale cloud and condensation scheme in the model is based on Tiedtke (1993), as described in Anderson et al. (2004), where other aspects of the models moist physics are described as well.

3. Results for AM2 physics

We have integrated the doubly periodic model for surface temperatures of 297, 299, 301, 303, and 305K. Figs. 2a and 2b are snapshots of the precipitation in equilibrated states at 301K and 305K respectively. The higher temperature case is distinguished by heavy precipitation spots not present in the colder case. We refer to these as "gridpoint storms" in the following, although they typically span several grid points in each direction. These are areas of predominantly large-scale condensation, as opposed to convective rainfall. Also shown in Figs. 2c and 2d are similar computations using a model with twice the resolution, for the temperatures 297 and 301K. A similar transition occurs in this higher resolution model, but at lower temperature.

Substantial changes in cloud forcing occur as one moves across this transition. Fig. 3 shows the fraction of precipitation that is large-scale (f_ℓ) as well as the total (short plus long wave) cloud-forcing (C_T), as a function of SSTs for the two resolutions. The changes in cloud forcing are in the sense of being strongly stabilizing, in that they result in stronger cooling to space as the SSTs warm. Away from the transition, C_T is only weakly sensitive to SST, possibly with a destabilizing, rather than stabilizing, slope. Longer integrations would be needed to define these weak slopes with more precision. The sensitivity to resolution in this model is the greatest for SSTs in the range at which gridpoint storms appear in the high resolution model but not at low resolution.

Also shown in Fig. 3c is a plot of C_T vs. f_ℓ. There is a tendency for the data to collapse onto a curve in this plane, suggesting that the variations in cloud forcing when the resolution is changed are, in fact, controlled in large part by the changes in the large-scale precipitation. This large-scale rain is not occurring in the model from thick "anvils" whose water is supplied by convection [as in the observations described by Houze (1989), for example]. Rather the water is upwelling directly from the lower troposphere on large scales in these non-rotating gridpoint storms.

In the full AM2p12 model, running over observed SSTs, the fraction of tropical (30N-30S) precipitation that is large-scale, as opposed to convective, is small, $\approx 5.3\%$. When one increases the SSTs by 2K everywhere and in all seasons, the large-scale fraction of tropical rain increases

to $\approx 7.3\%$. In the global warming simulations with CM2.0 (the coupled model using a slightly modified version of AM2p12 as an atmospheric component) the large-scale fraction of tropical rain is somewhat larger, but still increases with increasing temperature. In the IPCC A1B scenario (in which the CO_2 concentration increases to 720 ppm by 2100), for example, the increase is from 10% to 14% over the 21th century. Inspection of AM2 and CM2 shows that the tropical large-scale rain occurs primarily in rotating "tropical storms", and that this large-scale rain is once again supplied directly by upwelling of water from the lower troposphere on large scales.

CM2.0 has a fairly typical climate sensitivity: roughly 3K for the equilibrium response to doubling CO_2. If one assumed that the homogeneous, non-rotating results were directly relevant to the full model, one might expect that the sensitivity would decrease as tropical temperatures increased above 303K, due to negative cloud feedbacks associated with the increased "storminess". One sees no dramatic changes in sensitivity or in the total cloud forcing in the full model as the climate warms, presumably because the changes in f_ℓ in the full model are much smaller than in the radiative-convective simulations. However an experiment with quadrupled CO_2 over a slab-ocean lower boundary condition, which generates tropical ocean temperatures as large as 305K, shows a much larger increase in tropical storm activity than an experiment with only doubled CO_2 (J. Sirutis, personal communication), which we suspect is related to the transition seen in Fig. 3.

4. Varying the entrainment limiter

We now examine how the results for the 222 km version of the model are modified when we change the parameter α appearing in the definition of λ_0. We multiply the standard value $\alpha_* = 0.025$ by a factor of $0, 0+, 1, 2, 4$, and ∞. The first of these (0) consists of turning this entrainment limiter off. The second ($0+$) corresponds to eliminating only the non-entraining deep-convective plume. For $\alpha = \infty$ no deep convection can occur. SSTs are varied for each case. Results are shown in Fig. 4 with a similar format to that of Fig. 3. We also show in the figure the corresponding results for the tropical mean (ocean between 30N - 30S) of the global atmospheric

model in which α has been modified in the same way (experiments denoted on the top x-axis) and the result obtained when the SSTs in each of these models are increased uniformly by 2K.

When one reduces the strength of the entrainment rate limiter, or removes it entirely, the large-scale rain disappears entirely in the doubly periodic model, at least over this range of SSTs. For $\alpha > \alpha_*$, on the other hand, the transition to large-scale rain begins at a lower temperature. More limited experiments at the higher (111km) resolution (not shown) provide a similar picture. In particular, with $\alpha = \lambda_0 = 0$ there is little or no large scale precipitation in the high-resolution model over this SST range. As a result, there is much less sensitivity to horizontal resolution than with the standard value of α, consistent with the idea that much of this sensitivity is a result of the gridpoint storm generation.

As in Fig. 3, the (negative) cloud forcing in each case increases in magnitude as SSTs increase, with the cloud forcing interpolating between the relatively small cooling (20-25 $\mathrm{W\,m^{-2}}$) typical of cases with no large-scale rain and the much larger cooling (45-50 $\mathrm{W\,m^{-2}}$) generated by the model when the parameterized deep convection is completely inhibited. Plotting the results in the (C_T, f_ℓ) plane in Fig. 4c once again indicates that the large-scale fraction is the key aspect of the simulation that controls the cloud forcing as either SST or λ_0 are varied. The higher resolution results displayed in Fig. 3 fall close to this same curve. Varying other parameters in the convection scheme, particularly those that control precipitation efficiency, move the model off of this line.

In the global model simulations, f_ℓ increases and C_T becomes more negative as α increases, just as in the doubly-periodic model. The temperature sensitivity of f_ℓ is also qualitatively similar in the two models, especially for values of $\alpha/\alpha_* = 2$ and 4, for which the doubly-periodic model predicts that more of the tropics will reside in the temperature range over which f_ℓ is sensitive to SST. However, the temperature sensitivity of the total cloud forcing does not appear to be closely related to that in the homogeneous model, as the tropical mean C_T consistently becomes less negative with increasing SST in the global model.

Given the inhomogeneity of the tropics in the global model, one cannot easily assign the global model an effective SST for comparison with the uniform SST doubly periodic model.

But Fig. 4c indicates that we can predict how the cloud-forcing in the global model changes in response to changes in the entrainment limiter reasonably well, from the results of the doubly-periodic model, if we know the amount of large-scale precipitation in the global model. However, we cannot explain the relatively small changes in total cloud forcing due to the 2K increase in SST in this way.

Fig. 5 shows the individual short and long wave cloud forcings as functions of f_ℓ. The figure includes plots of the low level (p $>$ 700mb) cloudiness and the total condensed water as well. There is a large decrease in the longwave cloud forcing when one increases α from 0 to 0+; omission of the non-entraining plume decreases the upper level cloud amounts substantially. A similar result is found in the global model. For further increases in α, the long wave cloud forcing increases slowly, in both the global and radiative convective models, with the global model average over the tropics somewhat larger in each case.

For $\alpha > 0+$, the changes in cloud forcing are dominated by the shortwave component, with the negative cloud forcing increasing strongly with increasing f_ℓ, whether due to increasing α or increasing SST. The sensitivity of shortwave cloud forcing to f_ℓ is stronger in the radiative-convective than in the global model, but the qualitative behavior is the same.

The increase in low cloud cover with increasing gridpoint storminess is responsible for the increase in the magnitude of shortwave cloud forcing and can be seen in Fig. 5 as well. The dependence of tropical low cloud amount on α in the global model is captured rather well by the radiative-convective model, but once again the SST sensitivity is not. It is this increase in low cloud cover with increasing SST and f_ℓ in the radiative-convective model that results in the large, stabilizing, increase in the cloud forcing.

The behavior of the total condensate is especially simple when plotted in this way, with the condensate column increasing roughly linearly with f_ℓ in both models, although the global model tropics has more condensate than the radiative-convective model. The response to SST in the global model falls rather precisely on the same line as do the responses to variations in α.

Given the order-one inhomogeneity of the tropics and the effects of rotation, it is surprising

that there is this much similarity between the full model and a horizontally-homogeneous non-rotating model. Fig. 6 warns us not to expect too much in this regard. This figure shows changes in the mean temperature profile when one changes the entrainment limiter in the two models. In the GCM (Fig. 6a), there is a monotonic cooling of the troposphere as one changes the convection scheme so as to make it harder to generate deep convection. The case with no parameterized deep convection is as much as 5K colder at 200mb than the case with no constraint on entrainment rates. The analogous result for the radiative-convective model (Fig. 6b) is more complex. As α increases from 0 to $0+$, there is a large cooling of 2-3K in the upper troposphere, but then as α is increased further the troposphere warms. While we do not understand this result fully, it appears to be related to the variability of the surface winds and the associated variations in evaporation. This is suggested by the fact that the upper-level warming is accompanied by near surface warming and substantial changes in air-sea temperature differences. These temperature changes are associated with near surface mixing ratio changes of the same sense. It is a bit surprising that there is as much correspondence between the two models as there is, given this radically different response of the mean temperature profile.

To check that evaporation is involved in this discrepancy between the two models, we have added a constant to the wind speed that occurs in the model's surface flux computation:

$$|v| = (u^2 + v^2 + G^2)^{1/2} => (u^2 + v^2 + G^2 + G_*^2)^{1/2} \tag{1}$$

The model has a gustiness parameterization, G, proportional to the boundary layer convective velocity scale, which is present when the boundary layer is unstable and typically is of the order of 1 $\mathrm{m\,s^{-1}}$, but no parameterization of gustiness associated with convection. When we add a larger extra term ($G_* = 7\ \mathrm{m\,s^{-1}}$), we obtain the result in Fig. 6c from the radiative convective model. By weakening the connection between surface wind and evaporation, we can now mimic the monotonic behavior of the temperature profile in the GCM as a function of α. In fact, the temperature changes are now exaggerated, and one has the impression that $G*$ could be usefully

tuned to optimize this fit. (The model also develops more gridpoint noise in the vertical in the presence of this large surface wind enhancement, for reasons that are unclear.)

This result suggests that there may be systematic ways of modifying the radiative convective model to make its behavior correspond to the full GCM somewhat better, and that a candidate for this modification is the surface fluxes. These fluxes evidently are too sensitive to changes in convective organization in the radiative-convective model as compared to the full global model, due to the absence of larger scale flows.

5. Conclusions

We have placed the column physics of a GCM in a relatively simple, non-rotating, doubly periodic setting over fixed uniform SSTs, and compared some of the results with the tropical mean climate of the parent GCM. We vary the SSTs and a particular parameter that limits permissible entrainment rates in the plume model that underlies the convection scheme. We argue the case that this methodology helps us gain an important appreciation for some of the properties and peculiarities of a column physics model. Comparing the behavior of the column physics from different models in this idealized geometry would be educational.

Even if there were little direct correspondence between this homogeneous radiative-convective model and the tropics of the full GCM, understanding how different column physics packages behave in this idealized context could still be a useful stepping stone toward understanding the inhomogeneous, rotating case. The fact that there is some correspondence, at least in the model that we have examined (GFDL's AM2p12), is a bonus.

We have focused on the entrainment limiter in the convection scheme because it has a large effect on the model and, frankly, because we are concerned about the control that this parameter has on the full GCM solution and its sensitivity. There are a number of other aspects of the column physics that have interesting effects on the radiative-convective solution. We have seen a glimpse of the fact that the assumptions concerning gustiness at the surface are important in this model. There is also a sensitivity to parameters controlling precipitation efficiency that we have

not discussed here.

An important output statistic describing our homogeneous solutions is the fraction of precipitation that is large-scale rather than convective. Within the radiative-convective model, many of the effects of SST variations and variations in the entrainment limiter on total condensate, low cloud cover, and cloud forcing can be effectively described through their effect on this large-scale fraction. The response of the tropical mean of the full GCM and the radiative-convective model can also be made to look more similar by comparing solutions with the same values of this large-scale fraction, although we find that this works better for the changes in the entrainment rate limiter than for SST variations. Much of the difference between radiative-convective solutions with the two different horizontal resolutions examined can also be attributed to the increase in large-scale fraction with increasing resolution.

It is accepted that a substantial fraction of tropical rain does fall from large-scale anvils in convectively disturbed regions (Houze 1989). But the large-scale rainfall in the homogeneous solutions described here is not of this type. In observations, the water falling from anvils is supplied from the boundary layer by the convection. In our case, the rainfall in the gridpoint storms that play an important role in setting domain averaged properties is supplied from the boundary layer by the large-scale vertical motion itself, with little or no parameterized convection occurring within these storms.

A large-scale hydrostatic model of the tropics, if left to its own devices, organizes itself into gridpoint storms. The suggestion from the results described here is that the extent to which this tendency is suppressed by a particular convection scheme is essential to understanding how it affects the mean tropical climate. The doubly periodic geometry provides a clean framework for quantifying this suppression under controlled conditions.

One is led to ask what one ideally expects from a convection scheme in this regard. Our preconception is that at a resolution of 100-200 kms in a non-rotating geometry, it is reasonable to expect parameterized convection to suppress all gridpoint storms. AM2 column physics does not have this property; gridpoint storms form as one increases SSTs beyond 303K at 200km, and

beyond 297K at 100km resolution. Because it is difficult to make the handoff from convective to large-scale rain a smooth one, changes in this large-scale, gridpoint storm fraction can have significant effects on a model's climate response that may be undesirable.

On the other hand, the gridpoint storms in the doubly periodic model seem to be related to those in the full AM2 model, since some aspects of the model climates converge when plotted against the large-scale precipitation fraction. When we look at these gridpoint storms in the full AM2 model, they are rotating and their distribution bears some resemblance to the observed distribution of tropical storms, although AM2 is admittedly not particularly strong in this regard (J.Sirutis, personal communication). As we increase horizontal resolution to 100km and then 50km in AM2, the number of storms tends to increase but the distribution stays roughly the same, and individual storms begin to take on a more realistic character. If one changes the convection scheme by decreasing the entrainment limiter, one can eliminate nearly all tropical storms in AM2, just as one can eliminate the grid point storms in the radiative-convective model. From this perspective, it is not evident that elimination of all gridpoint storms is desirable.

Acknowledgments

We thank Drs. Steve Klein, Leo Donner, Steve Garner, Chris Bretherton, and Brian Mapes for useful discussions. Ming Zhao is supported under award NA17RJ2612 from the National Oceanic and Atmospheric Administration, U.S. Department of Commerce. The findings are those of the authors and do not necessarily reflect the views of the National Oceanic and Atmospheric Administration, or the U.S. Department of Commerce.

References

Anderson, J., V. Balaji, A. Broccoli, W. Cooke, T. Delworth, K. Dixon, L. Donner, K. Dunne, S. Freidenreich, S. Garner, R. Gudgel, C. Gordon, I. Held, R. Hemler, L. Horowitz, S. Klein, T. Knutson, P. Kushner, A. Langenhost, N.-C. Lau, Z. Liang, S. Malyshev, M. Nath, J. Ploshay, V. Ramaswamy, M. Schwarzkopf, E. Shevliakova, J. Sirutis, B. Soden, W. Stern, L. Thompson, McLean, R. Wilson, A. Wittenberg and B. Wyman, 2004: The new GFDL global atmosphere and land model AM2/LM2: Evaluation with prescribed SST simulations. *J. Climate*, **17**, 4641–4673.

Arakawa, A. and W. H. Schubert, 1974: Interaction of a cumulus cloud ensemble with the large-scale environment, Part I. *J. Atmos. Sci.*, **31**, 674–701.

Bretherton, C. S., P. N. Blossey and M. Khairoutdinov, 2005: An energy-balance analysis of deep convective self-aggregation above uniform SST. *J. Atmos. Sci., accepted for publication*.

Delworth, T., A. Broccoli, A. Rosati, R. Stouffer, V. Balaji, J. Beesley, W. Cooke, K. Dixon, J. Dunne, K. Dunne, J. Durachta, K. Findell, P. Ginoux, A. Gnanadesikan, C. Gordon, S. M. Briffies, R. Gudgel, M. Harrison, I. Held, R. Hemler, L. Horowitz, S. Klien, T. Knutson, P. J. Kushner, A. Langenhorst, H.-C. Lee, S.-J. Lin, J. Lu, S. Schwarzkopf, E. Shevliakova, J. Sirutis, M. Spelman, W. Stern, M. Winton, A. Wittenberg, B. Wyman, F. Zeng and R. Zhang, 2005: GFDL's CM2 global coupled climate models - Part I: Formulation and simulation characteristics. *J. Climate, accepted for publication*.

Held, I. R., R. S. Hemler and V. Ramaswamy, 1993: Radiative-convective equilibrium with explicit two-dimensional moist convection. *J. Atmos. Sci.*, **50**, 3909–3927.

Houze, J. R. A., 1989: Observed structure of mesoscale convective systems and implications for large-scale heating. *Q. J. R. Meteorol. Soc.*, **115**, 425–461.

Larson, K. and D. L. Hartmann, 2003: Interactions among cloud, water vapor, radiation, and large-scale circulation in the tropical climate. Part I: Sensitivity to uniform sea surface temperature changes. *Journal of Climate*, **16**, 1425–1440.

Moorthi, S. and M. J. Suarez, 1992: Relaxed Arakawa Schubert: A parameterization of moist convection for general circulation models. *Mon. Wea. Rev.*, **120**, 978–1002.

Tao, W.-K., J. Simpson, C.-L. Shie, B. Zhou, K. M. Lau and M. Moncrieff, 1999: Equilibrium states simulated by cloud-resolving models. *J. Atmos. Sci.*, pp. 3128–3139.

Tiedtke, M., 1993: Representation of clouds in large-scale models. *Mon. Wea. Rev.*, **121**, 3040–3061.

Tokioka, T., K. Yamazaki, A. Kitoh and T. Ose, 1988: The equatorial 30-60 day oscillation and the Arakawa-Schubert penetrative cumulus parameterization. *J. Meteor. Soc. Japan*, **66**, 883–901.

Tompkins, A. M. and G. C. Craig, 1999: Sensitivity of tropical convection to sea surface temperature in the absence of large-scale flow. *J. Climate*, **12**, 462–476.

Received October 10, 2005

With the extension package 'AGU^{++}', version 1.4a from 1996/07/29

Figure captions

Figure 1: a) A snapshot of the precipitation field ($\mathrm{mm\,day^{-1}}$) from a global radiative-convective equilibrium (GRCE) simulation. Rectangle represents the approximate domain size of the doubly periodic simulation in b). b) As in a) but from a doubly periodic radiative-convective equilibrium (DRCE) simulation.

Figure 2: a) A snapshot of the precipitation field ($\mathrm{mm\,day^{-1}}$) in equilibrated state from SST=301 K simulation. b) As in a) but for SST=305 K. c) As in a) but for SST=297 K and twice resolution (111 x 111 km) simulation. d) As in c) but for SST = 301 K.

Figure 3: a) Fraction of large-scale precipitation f_ℓ with respect to SSTs for AM2 default (circles) and twice resolution (triangles) simulations. b) As in a) but for total cloud forcing (C_T). c) Scatter plots of C_T versus f_ℓ. Solid lines connect individual experiments with varying SST (297, 299, 301, 303, 305 K). Filled symbols indicate the higher SST end.

Figure 4: a), b), c) are as in Fig. 3a, 3b, 3c respectively, but for the varying entrainment limiter experiments. Colors denote different choices of α/α_* (0, 0+, 1, 2, 4, and ∞). Triangles denote results for tropical mean of the global model experiments with the same modification of α (downward pointing triangles: control runs of global model denoted on the top x-axis; upward pointing triangles: as in the control runs except SSTs increased uniformly by 2 K).

Figure 5: As in Fig. 4c but for a) long wave cloud forcing, b) short wave cloud forcing, c) low cloud cover, d) total condensed water path.

Figure 6: a) The changes in tropical mean temperature profiles with α/α_* from global model simulations. b) As in a) but from standard doubly periodic simulations. c) As in b) but adding a constant G_* (7 $\mathrm{ms^{-1}}$) to wind speed in the model's surface flux calculation.

Figure Captions

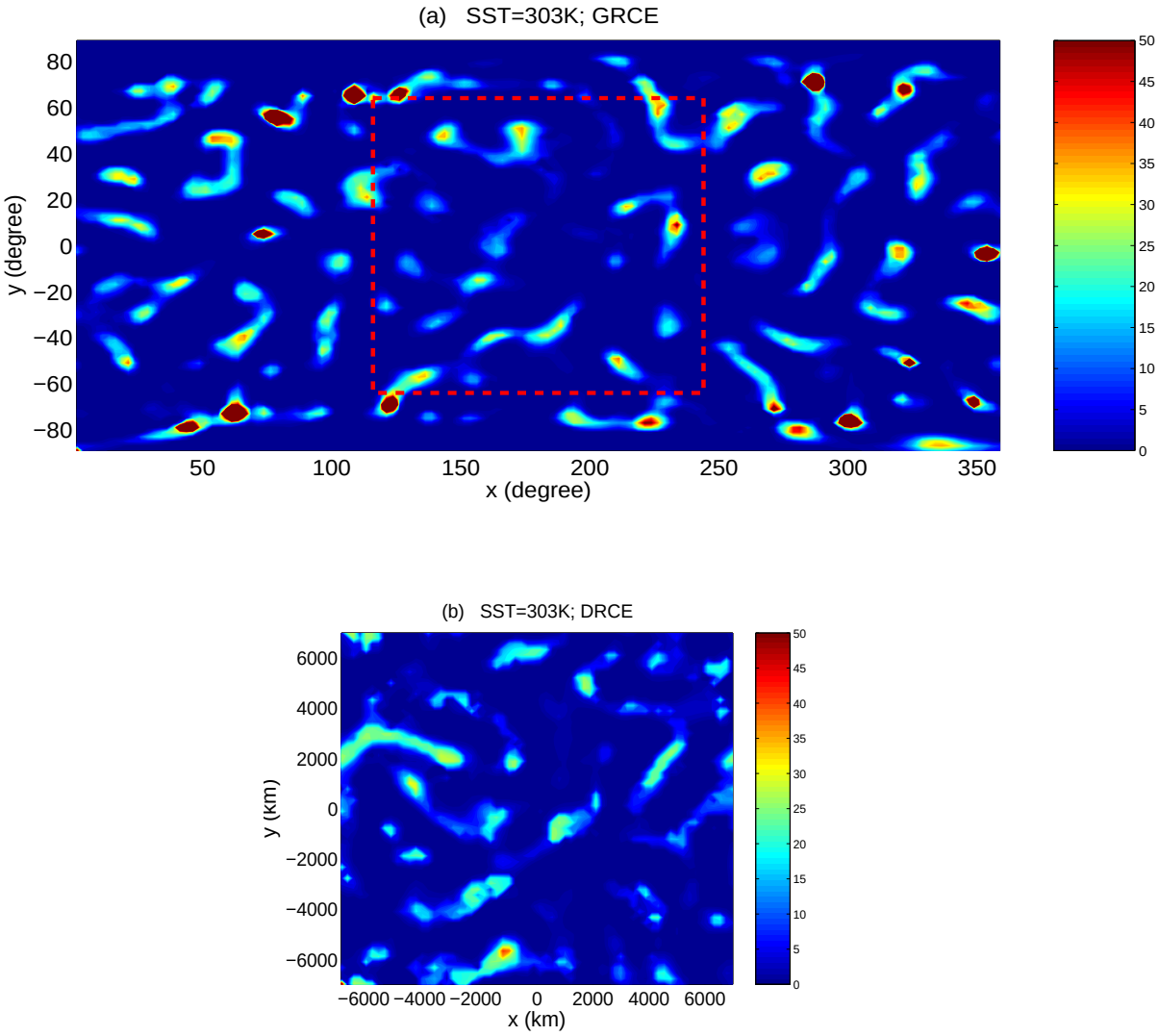

Figure 1. a) A snapshot of the precipitation field ($\mathrm{mm\,day^{-1}}$) from a global radiative-convective equilibrium (GRCE) simulation. Rectangle represents the approximate domain size of the doubly periodic simulation in b). b) As in a) but from a doubly periodic radiative-convective equilibrium (DRCE) simulation.

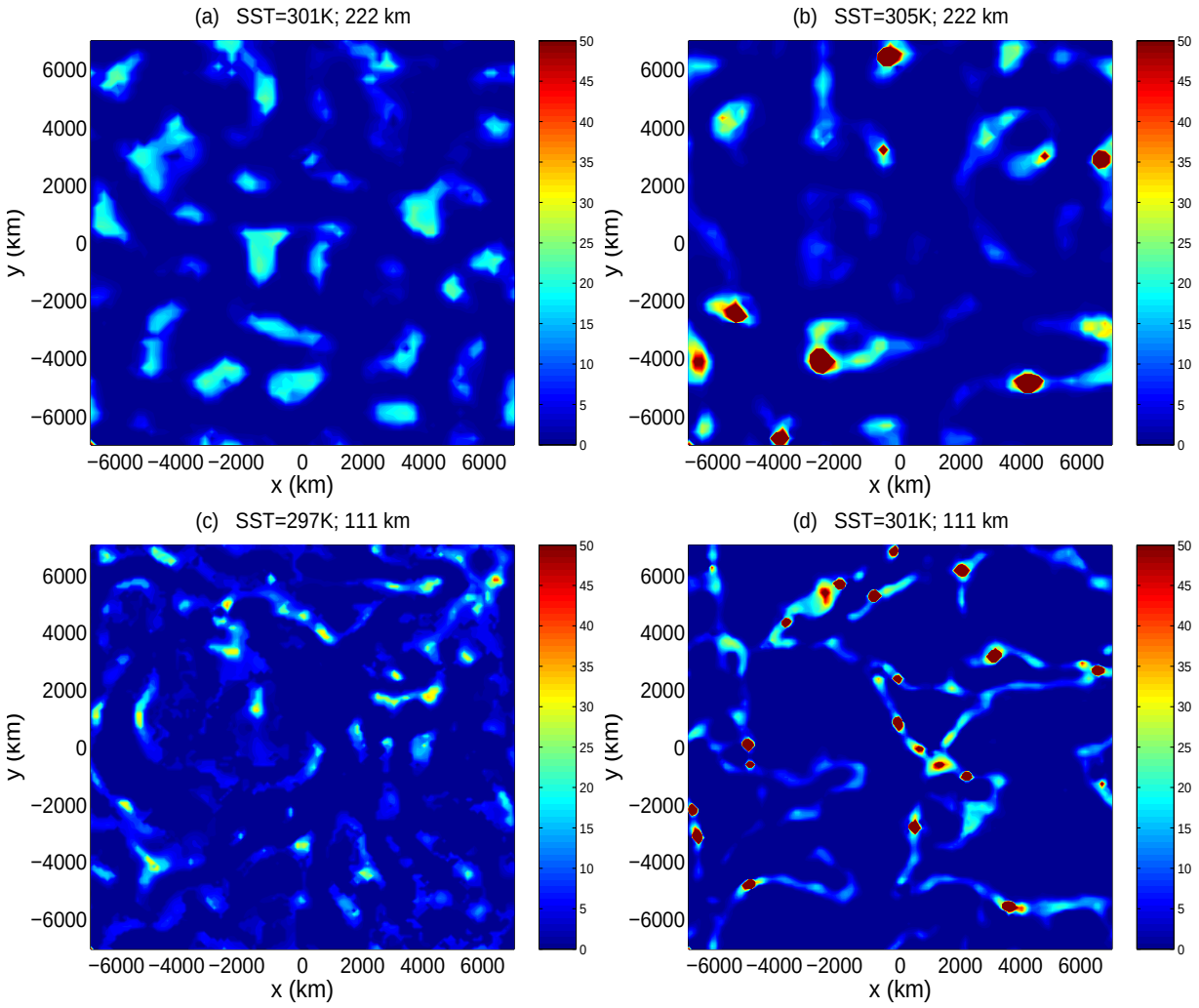

Figure 2. a) A snapshot of the precipitation field ($\mathrm{mm\,day^{-1}}$) in equilibrated state from SST=301 K simulation. b) As in a) but for SST=305 K. c) As in a) but for SST=297 K and twice resolution (111 x 111 km) simulation. d) As in c) but for SST = 301 K.

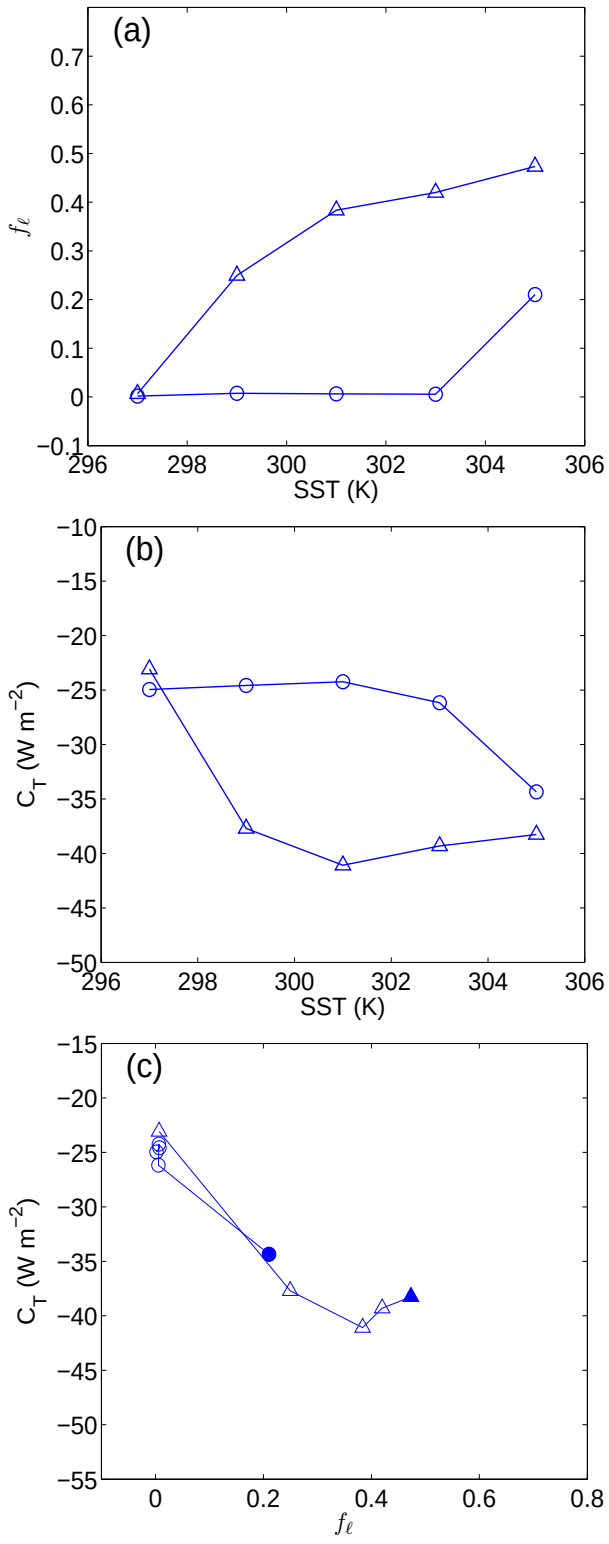

Figure 3. a) Fraction of large-scale precipitation f_ℓ with respect to SSTs for AM2 default (circles) and twice resolution (triangles) simulations. b) As in a) but for total cloud forcing (C_T). c) Scatter plots of C_T versus f_ℓ. Solid lines connect individual experiments with varying SST (297, 299, 301, 303, 305 K). Filled symbols indicate the higher SST end.

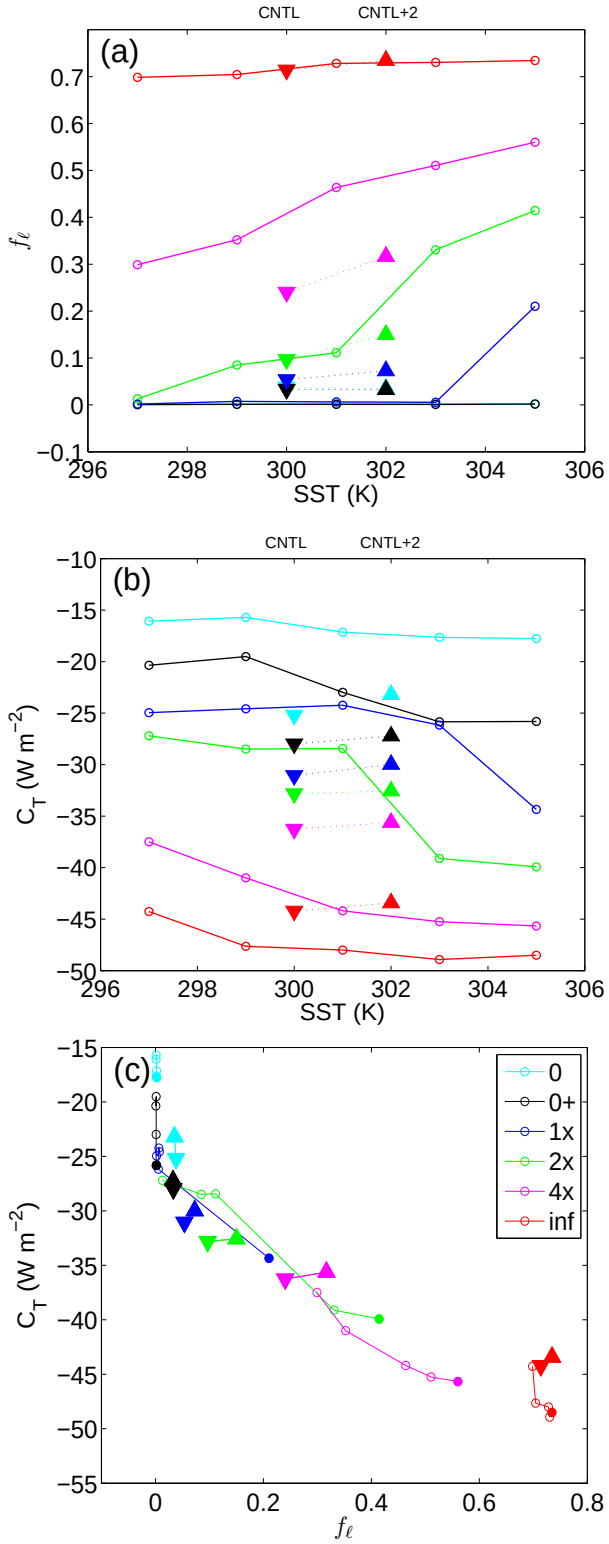

Figure 4. a), b), c) are as in Fig. 3a, 3b, 3c respectively, but for the varying entrainment limiter experiments. Colors denote different choices of α/α_* (0, 0+, 1, 2, 4, and ∞). Triangles denote results for tropical mean of the global model experiments with the same modification of α (downward pointing triangles: control runs of global model denoted on the top x-axis; upward pointing triangles: as in the control runs except SSTs increased uniformly by 2 K).

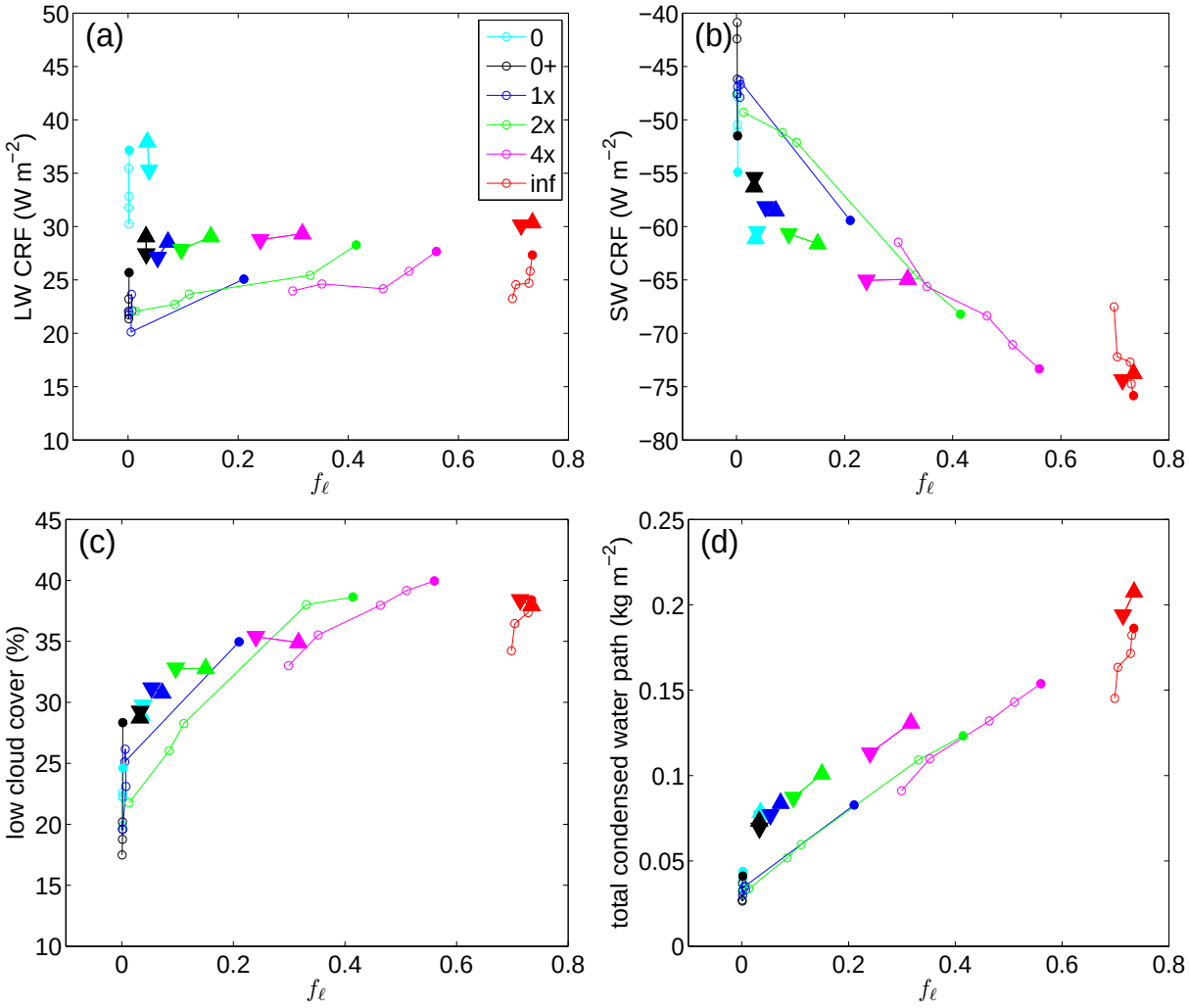

Figure 5. As in Fig. 4c but for a) long wave cloud forcing, b) short wave cloud forcing, c) low cloud cover, d) total condensed water path.

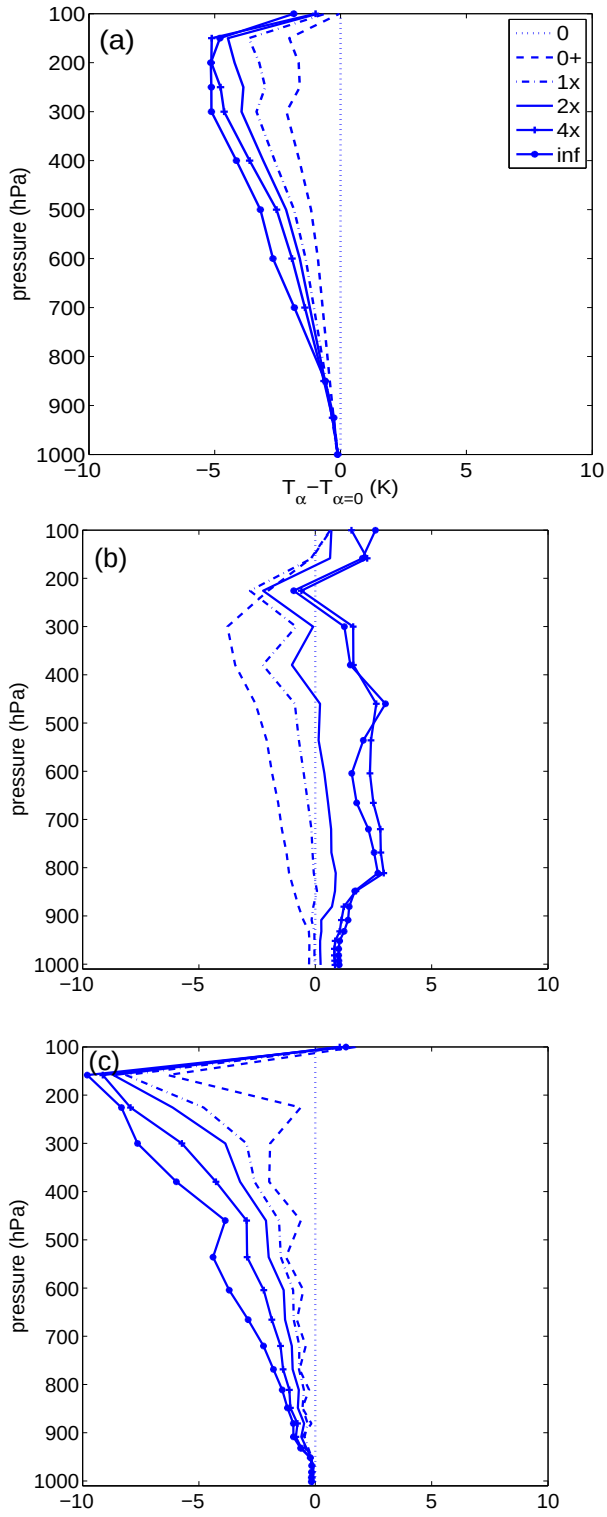

Figure 6. a) The changes in tropical mean temperature profiles with α/α_* from global model simulations. b) As in a) but from standard doubly periodic simulations. c) As in b) but adding a constant G_* (7 ms^{-1}) to wind speed in the model's surface flux calculation.